# Accepted Manuscript


Identification of novel inhibitors of histone acetyltransferase hMOF through high throughput screening

Rukang Zhang, Jiang Wang, Liang Zhao, Shien Liu, Daohai Du, Hong Ding, Shijie Chen, Liyan Yue, Yu-Chih Liu, Chenhua Zhang, Hong Liu, Cheng Luo

PII: S0223-5234(18)30690-1

DOI: 10.1016/j.ejmech.2018.08.026

Reference: EJMECH 10637

To appear in: *European Journal of Medicinal Chemistry*

Received Date: 13 April 2018

Revised Date: 25 July 2018

Accepted Date: 10 August 2018

Please cite this article as: R. Zhang, J. Wang, L. Zhao, S. Liu, D. Du, H. Ding, S. Chen, L. Yue, Y.-C. Liu, C. Zhang, H. Liu, C. Luo, Identification of novel inhibitors of histone acetyltransferase hMOF through high throughput screening, *European Journal of Medicinal Chemistry* (2018), doi: 10.1016/j.ejmech.2018.08.026.

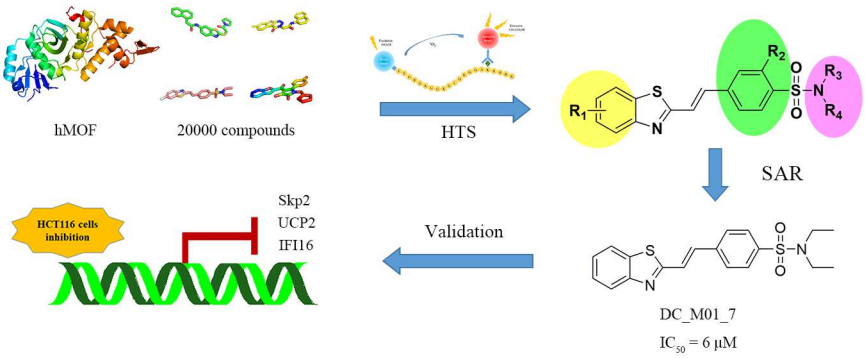

# Identification of novel inhibitors of histone acetyltransferase hMOF through high throughput screening

Rukang Zhang,[†,//,#] Jiang Wang,[†,#] Liang Zhao,[†] Shien Liu,[⊥] Daohai Du[†], Hong Ding[†], Shijie Chen[†], Liyan Yue[†], Yu-Chih Liu,[§] Chenhua Zhang,[§] Hong Liu,[*,†] and Cheng Luo[*,†]

†State Key Laboratory of Drug Research, CAS Key Laboratory of Receptor Research, Shanghai Institute of Materia Medica, Chinese Academy of Sciences, 555 Zuchongzhi Road, Shanghai 201203, China

[//]University of Chinese Academy of Sciences, 19 Yuquan Road, Beijing 100049, China

[⊥]WuXi AppTec, 288 Fute Zhong Road, Waigaoqiao Free Trade Zone, Shanghai 200131, China

[§]Shanghai ChemPartner Co., Ltd., #5 Building, 998 Halei Road, Shanghai 201203, China.

## ABSTRACT

The histone acetyltransferases (HATs) in mammals include GCN5 *N*-acetyltransferases, the MOZ, YBF2, SAS2, and TIP60 proteins, and the orphan HATs. The males absent on the first (MOF) is mainly related to acetylation of histone H4 Lys16 and has influence on downstream genes expression. However, the only inhibitor MG149 presented low activity against MOF. Besides, there was no high throughput screening platform on MOF, which limited the inhibitor discovery and functional study. In our study, we set up a high throughput screening platform based on amplified luminescent proximity homogeneous assay (ALPHA), which led us to a moderate inhibitor DC_M01. By chemical modification, we found DC_M01_7, which was the analog of DC_M01 with an $IC_{50}$ value of 6 μM. DC_M01_7 significantly inhibited HCT116 cells proliferation and could also inhibit histone 4 lysine 16 acetylation in HCT116 cells. To sum up, our work will probably assist the further development of more potent MOF inhibitors and the functional study of hMOF.

## HIGHLIGHT

- We identified a potent hMOF inhibitor with a new scaffold using high throughput screening.
- The binding affinity of the hit compound DC_M01 was measured by SPR.

- DC_M01_7, which was obtained by chemical modification, could inhibit hMOF activity in a substrate competitive mode.
- DC_M01_7 could inhibit hMOF activity in HCT116 cells and regulate downstream genes.

## KEYWORDS

High throughput screening; Epigenetics; Histone acetyltransferase; MOF; inhibitor;

## INTRODUCTION

Histone acetylation which gives rise to DNA relaxation with a positive influence on transcription can be regulated by histone acetyltransferases (HATs) and histone deacetylases (HDACs) [1]. Among these two kinds of enzymes, HATs can be divided into three groups, including the GNATs (Gcn5 N-acetyltransferases), the MOZ, YBF2, SAS2, and TIP60 proteins (MYSTs) and the orphan HATs [2]. MOF (males absent on the first), a member of the MYST family, was initially found to function by acetylation of histone H4 Lys16 (H4K16ac) in dosage compensation whereby transcription of genes on the single male X-chromosome must be increased two-fold relative to females who have two X-chromosomes [3, 4]. HMOF, the homolog of the Drosophila dosage compensation proteins MOF, forms human histone acetyltransferase complex (hMSL) which shows strong specificity for histone H4 lysine 16 in chromatin *in vitro* and *in vivo* [5].

HMOF displays quite diverse roles in various nuclear processes and some have also been implicated in carcinogenesis [6]. In comparison to normal tissues, hMOF is overexpressed in different kinds of cancers, such as human oral tongue squamous cell carcinoma (OTSCC), non-small cell lung cancer (NSCLC), colon cancer, and thymic lymphoma [7, 8]. In OTSCC, hMOF enhanced OSTCC growth by targeting EZH2 [9]. In lung cancer cells A549 and H1299, hMOF RNAi reduced the migration and adhesion. In addition, genes involved in cell proliferation, adhesion and migration like SKP2, ETS1 and ITAG2 were down-regulated. SKP2 is a subunit of SKP1-CUL1-F-box ubiquitin ligase complex that involved in regulation of G1 to S phase transition. The complex is also a positive regulator of proliferation [10]. Further experiments proved that hMOF promoted S phase entry via SKP2 in H1299 cells [8]. Another study revealed that hMOF mediated acetylation increased Nrf2 and its downstream genes and led to large tumor size, advanced disease stage and poor prognosis in NSCLC patients [11].

In breast cancer, MOF acetylated oncogene AIB1 and enhanced its function in promoting breast cancer cells [12]. Besides, in Hela cells, oncogene HOXA9, UCP2, KIAA0657, and HIP1 were down-regulated when cells were transfected with hMOF-specific siRNAs. Moreover, MOF depletion results in decreased cell numbers post-irradiation in SL-2 cells [13]. H4K16 acetylation had close relevance with breast cancer and colon cancer [14]. Analogs of SFN could sensitize HCT116 cells via modulate HAT/HDAC activities and associate DNA damage/repair signaling pathways [15]. Histone acetylation could upregulate the expression of NBL2 that was associate in colorectal cancer cells, such as HCT116 cells [16]. Another study showed that histone acetylation modulated the transcriptional activities of several tumor suppressors and immune modulatory genes that related in colorectal cancer cells [17]. Also, a recent study showed that deletion of MOF in a mouse model of MLL-AF9 driven leukemogenesis reduced tumor burden and prolonged host survival [18]. According to these data, we concluded hMOF inhibitor may find application in the treatment of several types of cancer such as leukemia, colon cancer, NSCLC. Therefore, searching for selective inhibitor of hMOF not only can facilitate researching hMOF function in related diseases but also may contribute to make promising tools for the treatment of diseases mentioned above.

Parallel to functional studies on HATs, researchers have aimed at developing small molecule inhibitors as chemical probes or potential therapeutic agents [19]. The current HAT inhibitors can be classified to three classes: bi-substrate, natural products, and novel small molecule inhibitors from virtual screening, high throughput screening or structure-based design [20]. The first bi-substrate inhibitor of HATs, H3-CoA-20 inhibitor was synthetized by Ronen Marmorstein's group at 2002 with an $IC_{50}$ value of 300 nM on tGCN5 [21]. In addition to bi-substrate analogs, several natural products have been reported as HAT inhibitors. Anacardic acid from cashewnut shell liquid and garcinol from Garcinia indica fruit rind were isolated by Kundu's group, which has inhibition on p300 and PCAF, respectively [22, 23]. Curcumin, a polyphenolic compound from curcuma longa rhizome, was shown to be a specific inhibitor of p300/CBP HAT activity with an $IC_{50}$ value of 25 μM [24]. However, unlike natural products, a limited number of novel small molecules have been described as HATi. MB-3 has been discovered as a GCN5 inhibitor with an $IC_{50}$ value of 100 μM [25]. Isothiazolones as

inhibitors of PCAF and p300 showed antiproliferative properties against a panel of human colon and ovarian tumor cell lines [26]. A series of garcinol analogues (the LTK compounds) has been reported as p300-specific HAT inhibitors ($IC_{50}$ values = 5-7 μM) but inactive for PCAF [27]. Quinoline derivatives have been described as HATi [28-30]. However, all these HATis reported have low selectivity and could not be made into drug due to their high toxicity and low-permeability.

As for hMOF inhibitor's study, Dekker and Zheng *et al.* synthesized MG149 (Figure 1) as an inhibitor of Tip60 and MOF which has an $IC_{50}$ value of 74 ± 20 μM and 47 ± 14 μM [31]. However, MG149 has no experimental data on hMOF in cell or *in vivo*. The lack of hMOF inhibitor limits the function study of hMOF and also restricts the treat of related diseases.

Amplified luminescent proximity homogeneous assay (ALPHA) donor beads produced approximately 60000 $^1O_2$ that can spread up to 200 nM to excite acceptor beads under 680 nM laser. ALPHA has become one of the most important methods in HTS due to its sensitivity, quickness and convenience [32-35]. In our study, we set up a high throughput screening (HTS) platform based on ALPHA and found a small molecule inhibitor DC_M01 of hMOF with an $IC_{50}$ value of 40 μM. The binding affinity of DC_M01 with hMOF is 19 μM *in vitro*. Then we synthesized a series of compounds based on DC_M01 and found the DC_M01_7, which inhibited hMOF *in vitro* with an $IC_{50}$ value of 6 μM. What's more, it can also dose-dependent inhibit hMOF in-cell. Taken together, our study indicates that DC_M01_7 and its analogs are new potential hMOF inhibitors, which exhibit the best inhibitory activity towards hMOF among all the reported hMOFi. This can provide us with new structural clues to develop more potent hMOF inhibitors and may help the function study of hMOF in future.

## RESULTS AND DISCUSSION

***High throughput screening based on ALPHA.***

As is mentioned before, the inhibitors of hMOF not only are in small quantity, but also have weak activity. Due to these reasons, we lack of small molecules for studying the function of hMOF and related diseases. To solve the problem of low efficiency of small molecule discovering, we set up a high throughput screening platform based on ALPHA (Figure S1). This is the first high throughput screening platform of hMOF which can probably accelerate the discovery of small molecule inhibitors

of hMOF even the function study of hMOF.

We screened our in-house small molecule library which contains more than 20000 compounds using this high throughput screening platform. The top 208 hit compounds from the first round screening were picked up and conducted the second round screening. After taking out the compounds with symmetrical structure and the compounds not suitable for structural modification, the hit DC_M01 with novel scaffold and best activity was picked up for further validation (Table S1).

***Radioactive acetylation Assay.***

To further validate the hit compounds, we performed radioactive acetylation assay and measured the hit compound previously mentioned. DC_M01 showed the activity with an $IC_{50}$ value of 40 μM (Figure 1). This result further proved that DC_M01, can inhibit hMOF activity *in vitro*. So we choose the hit DC_M01 to conduct further experiments for validation. In addition, the $IC_{50}$ value of MG149 was also measured in radioactive acetylation assay (Figure S2).

***Surface Plasmon Resonance (SPR) Based Binding Assay.***

To validate DC_M01 as a hMOF inhibitor, we used the SPR-based binding assay to measure the direct interaction between hMOF and DC_M01. The interactions of DC_M01 was dose-dependent and the equilibrium dissociation constant ($K_d$) is 19 μM (Figure 1). The $K_d$ of DC_M01 was consistent with the hMOF inhibition activity.

***Chemical Modification.***

To improve the inhibitory activity of human MOF (hMOF), a series of novel analogs DC_M01_1-DC_M01_7 was designed with incorporation of various substituents on the benzothiophene ring based on the structure of hit compound DC_M01. Then, DC_M01_8-DC_M01_15 were subsequently achieved *via* introducing various substituents to the phenyl ring and replacing the *N*,*N*-diethyl sulfonamide fragment with different sulfonamide while keeping the benzothiophene scaffold (Figure 2). The general synthetic route to DC_M01-DC_M01_12 is described in Scheme 1. Condensation of the commercially available substituted 2-methylbenzothiazole derivatives **2** and benzaldehyde **3** afforded the corresponding (*E*)-2-styryl benzothiazole **4**. Subsequently, compound **4** was reacted with excess chlorosulfonic acid to generate sulfonyl chlorides

**5**. Finally, the target molecules DC_M01-DC_M01_12 were obtained *via* condensation of sulfonyl chlorides **5** with different amines **6**. Compounds DC_M01_13- DC_M01_15 were synthesized according to Scheme 2. The intermidiate **8** was first afforded *via* condensation of sulfonyl chlorides **7** with diethylamine. Condensation of the commercially available 2-methylbenzo[d]thiazole **9** with formaldehyde gave the 2-vinylbenzo[d]thiazole **10**. Target compounds DC_M01_13-DC_M01_15 were generated by the coupling reaction of intermidiate **8** with 2-vinylbenzo[d]thiazole **10**.

***SAR Analysis.***

In order to assess the inhibitory activity of DC_M01_1-DC_M01_15 against hMOF, biochemical assays were performed as described in the experiment section. Compound potency against the hMOF was interrogated using MG149 as the positive control. The results were presented in Table 1. Firstly, hMOF inhibitory activity of the synthesized compounds that halogen was installed at the 5-position on the benzothiophene ring was tested. To our delight, compounds DC_M01, DC_M01_01, and -DC_M01_2 exhibited 53%, 64, and 57% hMOF inhibition at 50 μM, which displayed moderate inhibitory activities against hMOF with $IC_{50}$ values lower than 50. Introducing methyl (DC_M01_3) and methoxyl group (DC_M01_4) at the 5-position on the benzothiophene decreased the inhibitory activity. Compared with compound DC_M01_2, introduction of bromine (DC_M01_5) at the 6-position decreased the hMOF inhibitory activity. The mono-bromo substituted compounds (DC_M01_2 and DC_M01_5) demonstrated the regiochemical preference of the benzothiphene 5-position > 6-position. Compounds DC_M01_6 and DC_M01_7 exhibited good inhibitory activity with $IC_{50}$ values of 7.7 μM and 6 μM, which is better than the positive control MG149 ($IC_{50}$ = 15 μM). Then, the SAR at the sulfamide moiety was investigated. Replacement of *N*,*N*-diethyl sulfonamide moiety in DC_M01_7 with various sulfonamide afforded compounds DC_M01_8-DC_M01_12, which decreased the hMOF inhibitory activity. Finally, introduction of fluorine, chlorine, and methyl group at the 2-position of phenyl ring successively, compounds DC_M01_13-DC_M01_15 also decreased the hMOF inhibitory activity.

***Radioactive competitive assay.***

In order to identify the binding pocket of DC_M01_7, we conducted the radioactive competitive assay

to measure whether the DC_M01_7 could bind to the pocket of acetyl coenzyme A or the pocket of histone 4. The increase concentration of acetyl coenzyme A did not affect the inhibition of DC_M01_7 (Figure 3A). However, the increase concentration of histone 4 peptide decreased the activity of DC_M01_7. DC_M01_7 showed no inhibition on hMOF when the concentration of peptide was 10 μM (Figure 3B). This result illustrated that the DC_M01_7 inhibits hMOF by competitively occupying the binding pocket of histone 4.

**Docking Studies**

Based on the radioactive competitive assay, the binding pocket of compound DC_M01_07 was determined. Compounds DC_M01, DC_M01_6, DC_M01_7, and DC_M01_15 were selected to dock into the hMOF to investigate the binding modes and the interactions (Figure 4). It was observed that compound DC_M01 occupied the active binding pocket of histone 4 (Figure 4A). The *N*,*N*-diethyl sulfonamide moiety was forming hydrogen bonds with residues Ile144 and Ser181. Docking results showed that 4-fluorobenzothiazole formed extensive hydrophobic interactions with Aly101 (Fig. 4A). Compared with compound DC_M01, compounds DC_M01_6 and DC_M01_7 displayed the same binding mode with the active site of hMOF (Figures 4B and 4C). However, introduction of methyl group at the 2-position of phenyl ring, compound DC_M01_15 didn't form the hydrogen bond with Ile144, which is correlated with the decreased inhibitory activity (Figure 4D).

***Colony formation assay.***

According to previous study, hMOF in is overexpressed HCT116 cells.7 To investigate whether compound can inhibit the proliferation of cancer cells, so we chose HCT116 cells to conduct the colony formation assay. We used DC_M01_7 to treat HCT116 cells with different concentrations for 14 days and found that DC_M01_7 can dose-dependently inhibit the colony formation of HCT116 cells (Figure 5). However, the compound mg149 inhibits the colony formation only under concentration of 100 μM (Figure S4). This result indicated that DC_M01_7 led to cell death in HCT116 cells dose-dependently.

***HMOF in cell inhibition Assay.***

To confirm the DC_M01_7 can inhibit hMOF in cells, we conducted Western blot assays. After

treating HCT116 cells for 24 hours with SAHA and DC_M01_7, the histone 4 lysine 16 acetylation was measured using western blot assays. We observed a dose-dependently decrease of H4 lysine 16 acetylation (Figure 6A). This result demonstrated that DC_M01_7 could inhibit the hMOF activity because in cellular context hMOF is the only known enzyme to modify this site.

To further explore the antiproliferation mechanism of DC_M01_7, we examined whether the compound could block the oncogenes' expression in HCT116 cells. According to researches mentioned previously, hMOF knockdown leads to down-regulated of SKP2 and UCP2 that were regarded as oncogenes in cancer cells [7, 8, 36]. So we measured the compounds' effect on these genes' mRNA levels by using quantitative real-time PCR analysis. After treating HCT116 cells with DC_M01_7 for 3days, the mRNA levels of SKP2 and UCP2 were dose-dependent down-regulated. Meanwhile, the transcription level of IFI16 was up-regulated because IFI16 was reported to inhibit cell growth and mediate apoptosis by p53 pathway [37, 38] (Figure 6B).

## CONCLUSION

Histone acetylation catalyzed by HATs plays important roles in crucial cellular processes, such as embryonic development, DNA damage repairing, and it is also involved in cancer development. Most HAT inhibitors reported to date have low bioavailability. In our study, using the high throughput screening approach based on ALPHA technology, we identified DC_M01 as a novel inhibitor of hMOF with an $IC_{50}$ value of 40 μM. To validate the hit DC_M01, we then performed radioactive hMOF inhibition assay. To further confirm the binding mode of DC_M01 with hMOF, we conducted SPR experiments and the $K_d$ of DC_M01 was determined with 19 μM. After chemical modification, we synthesized a series of DC_M01's derivatives of which the DC_M01_7 has the $IC_{50}$ value of 6 μM. The DC_M01_7 also can led to cell death in HCT116 cells dose-dependently. To identify whether DC_M01_7 can work in cancer cells on hMOF, we detected the western blot assay and observed a dose-dependently decrease of H4 lysine 16 acetylation in HCT116 cells treated with DC_M01_7 in different concentrations. Also, the qPCR assay illustrated that DC_M01_7 could regulate the mRNA level of SKP2, UCP2, and IFI16.

Taken together, we found DC_M01_7 and its analogs are new hMOF inhibitors of which DC_M01_7

shows best activity with an $IC_{50}$ value of 6 μM. These compounds provided us with new structural clues to develop more potent hMOF inhibitors.

## EXPERIMENTAL SECTION

***Plasmid Construction, Protein Expression, and Purification.***

The plasmid was given as a gift by Ronen Marmorstein. The catalytic domain of hMOF (173-458) was cloned to pRSFBuetTEVa vector using BamH1 and Sal1 with an N-terminal hexahistidine (His6x) tag. The fusion protein was expressed in Escherichia coli BL21 (DE3) cells cultured at 37□ and was inducted at 16□ in the presence of 0.4 mM IPTG (isopropyl β-D-1-thiogalactopyranoside) when the OD600 reached 0.6. Cells were harvested 16 h and lysed by sonication in lysis buffer containing 20 mM HEPES (pH 7.4), 500 mM NaCl, 10 mM imidazole, 0.1% β-mercaptoethanol. The protein was first loaded on a HisTrap FF column (GE Healthcare), then washed using washing buffer (20 mM HEPES (pH 7.4), 5000 mM NaCl, 60 mM imidazole, 0.1% β-mercaptoethanol) and the fusion protein was eluted with elusion buffer (20 mM HEPES (pH 7.4), 500 mM NaCl , 350 mM imidazole , 0.1% β-mercaptoethanol). The eluted protein was purified further by Superdex75 column (GE Healthcare) in the buffer consisting 20 mM HEPES (pH 7.4), 200 mM NaCl, and 1 mM DTT. The purified protein was stored at -80 °C in buffer (20 mM HEPES (pH 7.4), 200 mM NaCl, 1 mM DTT, 5% glycerol).

***Radioactive hMOF Inhibition Assay.***

The radioactive hMOF acetylation inhibition assay was performed in 20 μL reaction system containing Acetyl Coenzyme A, [Acetyl-3H] - ([3H] Ac-CoA, 8.6 Ci/mmol, PerkinElmer), biotinylated H4 derived peptide (synthesized by GL China) and KAT8 (Produced by SIMM) in modified Tris Buffer, pH 7.5. The protein was pre-incubated with a range of compound concentrations for 15 min at room temperature before adding biotinylated peptide and [3H] Ac-CoA. After 240 min of incubation at room temperature, the reaction was stopped and was transferred to a 384-well streptavidin-coated Flashplate (PerkinElmer) and was incubated for another DC_M01_7 at room temperature. The Flashplate was washed with $dH_2O$ + 0.1% Tween-20 for three times and the radioactivity was determined by liquid scintillation counting (MicroBeta, PerkinElmer). $IC_{50}$ values were derived by fitting the data for the inhibition percentage to a dose-response curve by nonlinear

regression in GraphPad Prism 5.0.

***Surface Plasmon Resonance (SPR) Based Binding Assays.***

The SPR binding assays were performed on a Biacore T200 instrument (GE Healthcare) at 25 °C as described. HMOF protein was covalently immobilized on a CM5 chip using a standard amine-coupling procedure in 10 mM sodium acetate (pH 4.0). The chip was equilibrated with HBS buffer (20 mM HEPES (pH 7.4), 200 mM NaCl, 0.5% (v/v) DMSO). For kinetic measurement, compounds were diluted at concentrations ranging from 5 μM to 100 μM in HBS buffer. The diluted compounds were injected over the chip for 120 s at a flow rate of 30 μL/min and then dissociate for 300 s. The state model of the T200 evaluation software was used to analyze the resulting data to calculate the $K_d$ of the compounds.

***General Information.***

The reagents (chemicals) were purchased from commercial sources, and used without further purification. Analytical thin layer chromatography (TLC) was HSGF 254 (0.15-0.2 mm thickness). All products were characterized by their NMR and MS spectra. $^{1}H$ and $^{13}C$ NMR spectra were recorded on 400 MHz, 500 MHz, and 600 MHz instrument. Chemical shifts were reported in parts per million (ppm, δ) downfield from tetramethylsilane. Proton coupling patterns are described as singlet (s), doublet (d), triplet (t), quartet (q), doublet doublet (dd), multiplet (m). Low- and high-resolution mass spectra (LRMS and HRMS) were measured on spectrometer. HPLC analysis of all final biological testing compounds was carried out on an Agilent 1100 Series HPLC with an Agilent Extend-C18 column (150×4.6 mm, 5 μm). All final compounds achieved a minimum of 95% purity (Table S3).

***General procedure A: Synthesis of compounds DC_M01–DC_M01_12.***

(*E*)-5-fluoro-2-styrylbenzo[*d*]thiazole (**4a**)

To a mixture of 5-fluoro-2-methylbenzo[*d*]thiazole **2a** (224 mg, 1.34 mmol) and benzaldehyde **3** (142 mg 1.34 mmol) was added sodium amide (78 mg, 2 mmol) dissolved in dry DMF (5 mL), and the mixture was refluxed for 1 h. The reaction was cooled to ambient temperature, then the reaction solution was poured into ice-water (20 mL) to give crude product as yellow solid. The solid was subsequently recrystallized from ethanol to give (*E*)-5-fluoro-2-styrylbenzo[*d*]thiazole **4a**.

Yellow solid (232 mg, yield 68%): m.p. 121-125 °C. $^1$H NMR (400 MHz, DMSO-$d_6$) $\delta$ 8.11-8.06 (m, 1H), 7.97 (d, $J$ = 8.1 Hz, 1H), 7.78-7.74 (m, 2H), 7.70-7.58 (m, 2H), 7.54-7.48 (m, 1H), 7.45-7.40 (m, 2H). LRMS *m/z*: 256 $[M + H]^+$.

(*E*)-*N*,*N*-diethyl-4-(2-(5-fluorobenzo[*d*]thiazol-2-yl)vinyl)benzenesulfonamide (**DC_M01**).

(*E*)-5-fluoro-2-styrylbenzo[*d*]thiazole **DC_M01** (250 mg, 0.98 mmol) was added to a solution of the chlorosulfonic acid (3 mL) at 0°C for 5 minutes. The solution was stirred at room temperature for 8 h and then the mixture was poured into ice bath. Solid was precipitated and immediately collected without further purification. The yellow solid, that is sulfonyl chloride, was continuously reacted with diethylamine (98 mL, 9.8 mmol) in acetone. After 8 h, the mixture was poured into dilute hydrochloric acid and the resulting precipitate was filtered. The crude product was stirred in 1 M sodium hydroxide solution, and filtered as well followed by washing. The residue was purified by flash column chromatography (PE/EA = 10 : 1) to yield the desired product **DC_M01** (268 mg, yield 70%).

***General procedure B: Synthesis of compounds DC_M01_13–DC_M01_15.***

4-bromo-*N*,*N*-diethyl-2-fluorobenzenesulfonamide (**8n**)

To a solution of 4-bromo-2-fluorobenzene-1-sulfonyl chloride **7n** (100 mg, 0.37 mmol) in acetone (5 mL) was added diethylamine (270 mg, 3.7 mmol) dropwise. The mixture was stirred at ambient temperature for 5 h, and 1 *N* HCl (10 mL) was added to quench the reaction. The mixture was extracted with dichloromethane (20 mL) for three times, and the combined organic layer was washed with saturated $NaHCO_3$ solution and brine. The organic solution was subsequently dried over anhydrous $Na_2SO_4$ and concentrated *in vacuo*. The resulting residue was purified by flash column chromatography (PE/EA = 10 : 1) to give **8n**.

Pale yellow solid (103 mg, yield 90%): m.p. 68-71 °C, $^1$H NMR (400 MHz, $CDCl_3$) $\delta$ 7.71-7.58 (m, 4H), 3.23 (q, $J$ = 7.1 Hz, 4H), 1.13 (t, $J$ = 7.1 Hz, 6H). LRMS *m/z*: 310 $[M + H]^+$.

2-vinylbenzo[d]thiazole (**10**)

Formaldehyde (270 mg, 8.72 mmol), triethylamine (33.5 mg, 0.34 mmol), and diethylamine hydrochloride (790 mg, 8.72 mmol) were added to a solution of 2-methylbenzothiazole **9** (1.0 g, 6.71 mmol) in 1,4-dioxane (20 mL), and the mixture was stirred under 100 $^{o}$C for 4 h. Water was added and the mixture was extracted with dichloromethane (30 mL) for three times. The combined organic layer was washed with brine, dried over anhydrous $Na_2SO_4$ and concentrated under vacumn. The crude residue was purified by flash column chromatography (PE/EA = 50 : 1) to give compound **10**.

White solid (767 mg, yield 71%): m.p. 25-26 °C, $^1$H NMR (400 MHz, $CDCl_3$): $\delta$ 8.01-7.84 (m, 2H), 7.40-7.31 (m, 2H), 6.93 (dd, *J* = 16.8, 10.1 Hz, 1H), 5.93 (d, *J* = 13.8, Hz, 1H), 5.49 (dd, *J* = 16.7, 13.8 Hz, 1H). LRMS *m/z*: 161 $[M + H]^+$.

(*E*)-4-(2-(benzo[*d*]thiazol-2-yl)vinyl)-*N*,*N*-diethyl-2-fluorobenzenesulfonamide (**DC_M01_13**)

To a solution of 4-bromo-*N*,*N*-diethyl-2-fluorobenzenesulfonamide **8n** (100 mg, 0.32 mmol) in DMF (5 mL) was added 2-vinylbenzothiazole **10** (61.8 mg, 0.38 mmol). After all the solid was dissolved, palladium acetate (7.1 mg, 0.032 mmol), (±)-2,2'-bis(diphenylphosphino)-1,1'-binaphthalene (39.8 mg, 0.64 mmol), and $Et_3N$ (10 mg, 0.1 mmol) were added subsequently. The mixture was stirred at room temperature for 8 h. Water (20 mL) was added into the solution, and the mixture was extracted with dichloromethane (20 mL) for three times. The organic layer was separated, washed with brine, dried over anhydrous $Na_2SO_4$. The crud residue was purified by flash column chromatography (PE/EA = 10 : 1) to give **DC_M01_13** (75 mg, yield 60%).

*(E)-N,N*-diethyl-4-(2-(5-fluorobenzo[d]thiazol-2-yl)vinyl)benzenesulfonamide***(DC_M01)***.

Synthesized by following general procedure A: Yellow solid (268 mg, yield 70%): m.p. 195-198 °C. $^1$H NMR (400 MHz, DMSO-$d_6$) $\delta$ 8.19 (dd, *J* = 8.9, 5.3 Hz, 1H), 8.01 (d, *J* = 8.3 Hz, 2H), 7.89-7.82 (m, 3H), 7.81-7.79 (m, 2H), 7.42-7.36 (m, 1H), 3.20 (q, *J* = 7.1 Hz, 4H), 1.06 (t, *J* = 7.1 Hz, 6H). $^{13}$C NMR (125 MHz, DMSO-$d_6$) $\delta$ 168.5, 161.4, (d, *J* = 243.6 Hz), 154.2, 140.0, 139.0, 135.8, 130.2, 128.4, 127.2, 124.3, 123.7, 114.2, 108.5, 41.8, 14.1. ESI-MS *m/z*: 391 $[M + H]^+$. ESI-HRMS calcd for $C_{19}H_{20}FN_2O_2S_2$ $[M + H]^+$ 391.0945, found 391.0949.

*(E)-4-(2-(5-chlorobenzo[d]thiazol-2-yl)vinyl)-N,N-diethylbenzenesulfonamide(**DC_M01_1**).*

Synthesized by following general procedure A: Yellow solid (262 mg, yield 70%): m.p. 291-294 °C. $^{1}$H NMR (400 MHz, DMSO-$d_6$) $\delta$ 8.21 (d, $J$ = 1.9 Hz, 1H), 8.11 (d, $J$ = 8.5 Hz, 1H), 7.99 (d, $J$ = 8.6 Hz, 2H), 7.84-7.80 (m, 2H), 7.74 (d, $J$ = 8.3 Hz, 1H), 7.65-7.62 (m, 1H), 7.62-7.60 (m, 1H), 3.17 (q, $J$ = 7.1 Hz, 4H), 1.03 (t, $J$ = 7.1 Hz, 6H). $^{13}$C NMR (125 MHz, DMSO-$d_6$) $\delta$ 167.9, 154.6, 140.0, 139.0, 136.2, 133.5, 128.5, 127.2, 126.1, 125.0, 124.3, 124.1, 119.4, 41.8, 14.1. ESI-MS *m/z*: 407 $[M + H]^+$. ESI-HRMS calcd for $C_{19}H_{20}ClN_2O_2S_2$ $[M + H]^+$ 407.0649, found 407.0654.

*(E)-4-(2-(5-bromobenzo[d]thiazol-2-yl)vinyl)-N,N-diethylbenzenesulfonamide(**DC_M01_2**).*

Synthesized by following general procedure A: Yellow solid (236 mg, yield 66%): m.p. 175-178 °C. $^{1}$H NMR (400 MHz, DMSO-$d_6$) $\delta$ 8.45 (d, $J$ = 2.0 Hz, 1H), 8.01 (d, $J$ = 8.2 Hz, 2H), 7.95 (d, $J$ = 8.7 Hz, 1H), 7.84 (d, $J$ = 8.2 Hz, 2H), 7.80 (s, 2H), 7.70 (dd, $J$ = 8.7, 2.1 Hz, 1H), 3.20 (q, $J$ = 7.1 Hz, 4H), 1.06 (t, $J$ = 7.1 Hz, 6H). $^{13}$C NMR (125 MHz, DMSO-$d_6$) $\delta$ 166.8, 152.4, 140.0, 139.1, 136.3, 136.0, 129.8, 128.4, 127.2, 124.9, 124.3, 124.2, 118.3, 41.8, 14.1. ESI-MS *m/z*: 451 $[M + H]^+$. ESI-HRMS calcd for $C_{19}H_{20}BrN_2O_2S_2$ $[M + H]^+$ 451.0144, found 451.0156.

*(E)-N,N-diethyl-4-(2-(5-methylbenzo[d]thiazol-2-yl)vinyl)benzenesulfonamide (**DC_M01_3**).*

Synthesized by following general procedure A: Yellow solid (278 mg, yield 72%): m.p. mp 256-270 °C. $^{1}$H NMR (400 MHz, DMSO-$d_6$) $\delta$ 7.97 (d, $J$ = 8.6 Hz, 2H), 7.88 (d, $J$ = 8.3 Hz, 1H), 7.83-7.79 (m, 2H), 7.72 (d, $J$ = 10.6 Hz, 2H), 7.57-7.63 (m, 1H), 7.37-7.32 (m, 1H), 3.17 (q, $J$ = 7.1 Hz, 4H), 2.44 (s, 3H), 1.03 (t, $J$ = 7.1 Hz, 6H). $^{13}$C NMR (125 MHz, DMSO-$d_6$) $\delta$ 164.7, 151.6, 139.7, 139.2, 135.6, 134.9, 134.4, 128.2, 127.2, 126.1, 124.7, 122.3, 121.8, 41.8, 21.1, 14.1. ESI-MS *m/z*: 387 $[M + H]^+$. ESI-HRMS calcd for $C_{20}H_{23}N_2O_2S_2$ $[M + H]^+$ 387.1195, found 387.1200.

*(E)-N,N-diethyl-4-(2-(5-methoxybenzo[d]thiazol-2-yl)vinyl)benzenesulfonamide (**DC_M01_4**).*

Synthesized by following general procedure A: Yellow solid (248 mg, yield 66%): m.p. 163-165 °C.

$^{1}$H NMR (400 MHz, DMSO-$d_6$) $\delta$ 8.00 (dd, $J$ = 8.6, 1.9 Hz, 3H), 7.83 (d, $J$ = 8.3 Hz, 2H), 7.75 (d, $J$ = 5.1 Hz, 2H), 7.55 (d, $J$ = 2.5 Hz, 1H), 7.12 (dd, $J$ = 8.8, 2.5 Hz, 1H), 3.87 (s, 3H), 3.20 (q, $J$ = 7.0 Hz, 4H), 1.06 (t, $J$ = 7.1 Hz, 6H). $^{13}$C NMR (125 MHz, DMSO-$d_6$) $\delta$ 166.8, 158.9, 154.8, 139.8, 139.2, 134.8, 128.3, 127.2, 126.1, 124.7, 122.6, 115.5, 105.4, 55.5, 41.8, 14.1. ESI-MS *m/z*: 403 $[M + H]^+$. ESI-HRMS calcd for $C_{20}H_{23}N_2O_3S_2$ $[M + H]^+$ 403.1145, found 403.1134.

*(E)-4-(2-(6-bromobenzo[d]thiazol-2-yl)vinyl)-N,N-diethylbenzenesulfonamide (**DC_M01_5**).*

Synthesized by following general procedure A: Yellow solid (232 mg, yield 65%): m.p. 167-168 °C. $^{1}$H NMR (500 MHz, DMSO-$d_6$) $\delta$ 8.55-8.53 (m, 1H), 8.10 (d, $J$ = 8.2 Hz, 2H), 8.04 (d, $J$ = 8.7 Hz, 1H), 7.93 (d, $J$ = 8.2 Hz, 2H), 7.88 (s, 2H), 7.81-7.77 (m, 1H), 3.30 (q, $J$ = 7.1 Hz, 4H), 1.15 (t, $J$ = 7.1 Hz, 6H). $^{13}$C NMR (125 MHz, DMSO-$d_6$) $\delta$ 167.9, 154.6, 140.0, 139.0, 136.2, 133.5, 128.5, 128.4, 127.2, 125.0, 124.2, 124.1, 119.4, 41.8, 14.1. ESI-MS *m/z*: 451 $[M + H]^+$. ESI-HRMS calcd for $C_{19}H_{20}BrN_2O_2S_2$ $[M + H]^+$ 451.0144, found 451.0142.

*(E)-4-(2-(5,6-dimethylbenzo[d]thiazol-2-yl)vinyl)-N,N-diethylbenzenesulfonamide (**DC_M01_6**).*

Synthesized by following general procedure A: Yellow solid (272 mg, yield 72%): m.p. 201-206 °C. $^{1}$H NMR (400 MHz, DMSO-$d_6$) $\delta$ 7.98 (d, $J$ = 8.3 Hz, 2H), 7.89-7.77 (m, 4H), 7.75-7.68 (m, 2H), 3.20 (q, $J$ = 7.1 Hz, 4H), 2.37 (s, 6H), 1.06 (t, $J$ = 7.1 Hz, 6H). $^{13}$C NMR (125 MHz, DMSO-$d_6$) $\delta$ 164.5, 152.2, 139.7, 139.3, 135.6, 135.2, 134.6, 131.7, 128.2, 127.2, 124.9, 122.8, 121.8, 41.8, 19.7, 14.1. ESI-MS *m/z*: 401 $[M + H]^+$. ESI-HRMS calcd for $C_{21}H_{25}N_2O_2S_2$ $[M + H]^+$ 401.1352, found 401.1349.

*(E)-4-(2-(benzo[d]thiazol-2-yl)vinyl)-N,N-diethylbenzenesulfonamide (**DC_M01_7**).*

Synthesized by following general procedure A: Yellow solid (251 mg, yield 64%): m.p. 189-192 °C. $^{1}$H NMR (500 MHz, DMSO-$d_6$) $\delta$ 8.15-8.12 (m, 1H), 8.04-7.99 (m, 3H), 7.85-7.81 (m, 2H), 7.79-7.76 (m, 2H), 7.57– 7.53 (m, 1H), 7.49-7.45 (m, 1H), 3.20 (q, $J$ = 7.1 Hz, 4H), 1.06 (t, $J$ = 7.1 Hz, 6H). $^{13}$C NMR (125 MHz, DMSO-$d_6$) $\delta$ 165.8, 153.4, 139.8, 139.2, 135.4, 134.3, 128.3, 127.2, 126.6, 125.7, 124.6, 122.7, 122.3, 41.8, 14.1. ESI-MS *m/z*: 373 $[M + H]^+$. ESI-HRMS calcd for $C_{19}H_{21}N_2O_2S_2$ [M +

H]$^+$ 373.1039, found 373.1041.

*(E)-4-(2-(benzo[d]thiazol-2-yl)vinyl)-N,N-dimethylbenzenesulfonamide (**DC_M01_8**)*

Synthesized by following general procedure A: Yellow solid (271 mg, yield 58%): m.p. 208-211 °C. $^1$H NMR (400 MHz, DMSO-$d_6$) $\delta$ 8.14 (d, $J$ = 7.9 Hz, 1H), 8.08-8.00 (m, 3H), 7.86 -7.74 (m, 4H), 7.58-7.51 (m, 1H), 7.50 -7.45 (m, 1H), 2.64 (s, 6H). $^{13}$C NMR (125 MHz, DMSO-$d_6$) $\delta$ 165.7, 153.4, 139.6, 135.3, 134.8, 134.3, 128.3, 128.0, 126.7, 125.8, 124.8, 122.8, 122.3, 37.6. ESI-MS *m/z*: 345 [M + H]$^+$. ESI-HRMS calcd for $C_{17}H_{17}N_2O_2S_2$ [M + H]$^+$ 345.0726, found 345.0717.

*(E)-4-(2-(benzo[d]thiazol-2-yl)vinyl)-N-phenylbenzenesulfonamide (**DC_M01_9**)*

Synthesized by following general procedure A: Yellow solid (267 mg, yield 70%): m.p. 209-213 °C. $^1$H NMR (400 MHz, DMSO-$d_6$) $\delta$ 10.33 (s, 1H), 8.12 (d, $J$ = 7.9 Hz, 1H), 8.00 (d, $J$ = 8.1 Hz, 1H), 7.93 (d, $J$ = 8.2 Hz, 2H), 7.80-7.65 (m, 4H), 7.53 (t, $J$ = 7.6 Hz, 1H), 7.46 (t, $J$ = 7.5 Hz, 1H), 7.24 (t, $J$ = 7.8 Hz, 2H), 7.14-7.09 (m, 2H), 7.03 (t, $J$ = 7.4 Hz, 1H). $^{13}$C NMR (125 MHz, DMSO-$d_6$) $\delta$ 165.7, 153.4, 139.5, 139.4, 137.6, 135.3, 134.2, 129.2, 128.2, 127.2, 126.6, 125.7, 124.7, 124.2, 122.8, 122.3, 120.2. ESI-MS *m/z*: 391 [M - H]$^-$. ESI-HRMS calcd for $C_{21}H_{15}N_2O_2S_2$ [M - H]$^-$ 391.0580, found 391.0588.

*(E)-4-(2-(benzo[d]thiazol-2-yl)vinyl)-N-benzylbenzenesulfonamide (**DC_M01_10**)*

Synthesized by following general procedure A: Yellow solid (263 mg, yield 70%): m.p. 225-229 °C. $^1$H NMR (400 MHz, DMSO-$d_6$) $\delta$ 8.27-8.22 (m, 1H), 8.15 (d, $J$ = 7.9 Hz, 1H), 8.05-7.96 (m, 3H), 7.81 (dd, $J$ = 23.1, 7.3 Hz, 4H), 7.59-7.53 (m, 1H), 7.51-7.45 (m, 1H), 7.33-7.20 (m, 5H), 4.03 (d, $J$ = 6.2 Hz, 2H). $^{13}$C NMR (125 MHz, DMSO-$d_6$) $\delta$ 165.8, 153.4, 140.8, 138.9, 137.6, 135.5, 134.2, 128.2, 128.2, 127.6, 127.1, 127.0, 126.7, 125.7, 124.4, 122.7, 122.3, 46.1. ESI-MS *m/z*: 405 [M - H]$^-$. ESI-HRMS calcd for $C_{22}H_{17}N_2O_2S_2$ [M - H]$^-$ 405.0737, found 405.0740.

*(E)-4-(2-(benzo[d]thiazol-2-yl)vinyl)-N-(4-methylbenzyl)benzenesulfonamide (**DC_M01_11**)*

Synthesized by following general procedure A: Yellow solid (195 mg, yield 53%): m.p. 199-202 °C, HPLC: 99.8%. $^{1}$H NMR (400 MHz, DMSO-$d_6$) $\delta$ 8.13 (d, $J$ = 7.8 Hz, 2H), 8.02 (d, $J$ = 8.1 Hz, 1H), 7.98-7.94 (m, 2H), 7.83-7.75 (m, 4H), 7.58-7.52 (m, 1H), 7.50 -7.44 (m, 1H), 7.14 (d, $J$ = 8.5 Hz, 2H), 6.86-6.80 (m, 2H), 3.94 (s, 2H), 3.70 (s, 3H). $^{13}$C NMR (125 MHz, DMSO-$d_6$) $\delta$ 165.8, 158.4, 153.4, 140.9, 138.8, 135.5, 134.2, 129.3, 128.9, 128.1, 127.0, 126.6, 125.7, 124.4, 122.7, 122.3, 113.6, 55.0, 45.7. ESI-MS *m/z*: 419 [M - H]$^-$. ESI-HRMS calcd for $C_{23}H_{19}N_2O_2S_2$ [M - H]$^-$ 419.0899, found 419.0902.

*(E)-4-(2-(benzo[d]thiazol-2-yl)vinyl)-N-(4-methoxyphenyl)benzenesulfonamide (**DC_M01_12**)*

Synthesized by following general procedure A: Yellow solid (199 mg, yield 55%): m.p. 197-200 °C. $^{1}$H NMR (400 MHz, DMSO-$d_6$) $\delta$ 8.20-8.10 (m, 2H), 8.01 (d, $J$ = 8.2 Hz, 1H), 7.98 -7.40 (m, 2H), 7.83-7.79 (m, 2H), 7.79-7.71 (m, 2H), 7.58-7.51 (m, 1H), 7.49-7.44 (m, 1H), 7.09 (q, $J$ = 8.1 Hz, 4H), 3.96 (d, $J$ = 6.2 Hz, 2H), 2.24 (s, 3H). $^{13}$C NMR (125 MHz, DMSO-$d_6$) $\delta$ 165.8, 153.4, 140.9, 138.9, 136.3, 135.5, 134.4, 134.2, 128.7, 128.1, 127.6, 127.0, 126.6, 125.7, 124.4, 122.7, 122.3, 45.9, 20.6. ESI-MS *m/z*: 435 [M - H]$^-$. ESI-HRMS calcd for $C_{23}H_{19}N_2O_3S_2$ [M - H]$^-$ 435.0843, found 435.0834.

*(E)-4-(2-(benzo[d]thiazol-2-yl)vinyl)-N,N-diethyl-2-fluorobenzenesulfonamide (**DC_M01_13**)*

Synthesized by following general procedure B: Yellow solid (75 mg, yield 60%): m.p. 180-185 °C. $^{1}$H NMR (400 MHz, DMSO-$d_6$) $\delta$ 8.42 (d, $J$ = 8.4 Hz, 1H), 8.17 (d, $J$ = 8.2 Hz, 2H), 8.12-8.08 (m, 1H), 8.06-8.05 (m, 1H), 7.98-7.87 (m, 2H), 7.61-7.55 (m, 1H), 7.54-7.48 (m, 1H), 3.25 (q, $J$ = 7.0 Hz, 4H), 1.09 (t, $J$ = 7.1 Hz, 6H). $^{13}$C NMR (125 MHz, DMSO-$d_6$) $\delta$ 164.6, 153.3, 140.2, 137.4, 134.6, 130.9, 129.5, 128.9, 128.4, 126.9, 126.0, 124.2, 123.1, 122.4, 42.0, 14.2. ESI-MS *m/z*: 391 [M + H]$^+$. ESI-HRMS calcd for $C_{19}H_{20}FN_2O_2S_2$ [M + H]$^+$ 391.0945, found 391.0946.

*(E)-4-(2-(benzo[d]thiazol-2-yl)vinyl)-2-chloro-N,N-diethylbenzenesulfonamide (**DC_M01_14**)*

Synthesized by following general procedure B Yellow solid (86 mg, yield 55%): m.p. 168-171 °C. $^{1}$H NMR (500 MHz, DMSO-$d_6$) $\delta$ 8.16-8.13 (m, 2H), 8.05-7.99 (m, 2H), 7.96-7.92 (m, 1H), 7.89 (d, $J$ =

16.2 Hz, 1H), 7.74 (d, *J* = 16.2 Hz, 1H), 7.58-7.52 (m, 1H), 7.51-7.48 (m, 1H), 3.34 (q, *J* = 7.1 Hz, 4H), 1.07 (t, *J* = 7.1 Hz, 6H). $^{13}$C NMR (125 MHz, DMSO-$d_6$) $\delta$ 165.4, 153.4, 140.9, 137.5, 134.4, 133.9, 131.4, 131.3, 130.6, 126.7, 126.3, 125.9, 125.8, 122.8, 122.3, 41.2, 13.9. ESI-MS *m/z*: 407 [M + H]$^+$. ESI-HRMS calcd for $C_{19}H_{20}ClN_2O_2S_2$ [M + H]$^+$ 407.0649, found 407.0647.

*(E)-4-(2-(benzo[d]thiazol-2-yl)vinyl)-N,N-diethyl-2-methylbenzenesulfonamide (**DC_M01_15**)*

Synthesized by following general procedure B: Yellow solid (80 mg, yield 54%): m.p. 140-145 °C. $^1$H NMR (500 MHz, DMSO-$d_6$) $\delta$ 8.15-8.12 (m, 1H), 8.04-8.00 (m, 1H), 7.88-7.86 (m, 1H), 7.84-7.76 (m, 3H), 7.69 (d, *J* = 16.2 Hz, 1H), 7.57-7.53 (m, 1H), 7.49-7.45 (m, 1H), 3.28 (q, *J* = 7.1 Hz, 4H), 2.57 (s, 3H), 1.07 (t, *J* = 7.1 Hz, 6H). $^{13}$C NMR (125 MHz, DMSO-$d_6$) $\delta$ 165.8, 153.4, 139.1, 138.6, 137.3, 135.3, 134.2, 131.6, 129.2, 126.6, 125.7, 125.3, 124.5, 122.7, 122.3, 40.8, 19.8, 13.8. ESI-MS *m/z*: 387 [M + H]$^+$. ESI-HRMS calcd for $C_{20}H_{23}N_2O_2S_2$ [M + H]$^+$ 387.1195, found 387.1192.

***Molecular docking***

All the available crystal structures of hMOF (2GIV, 2PQ8, 2Y0M, 2Y0N, 3QAH, 3TOA, 3TOB, 4DNC, 5J8C, 5J8F) were superimposed and the local flexibility of the residues around the cofactor COA were observed when we checked the aligned structures. In order to rescue the poorly scored compounds from standard virtual docking studies, Induced Fit Docking (IFD) protocol was selected to predict the biding mode of the investigated compounds with relatively high activity against hMOF. The X-ray structure of hMOF with both substrates and high resolution (PDB code 2GIV) among these determined hMOF X-ray structures was fetched from PDB Web site and was prepared using default protocol of the Protein Preparation Wizard (Schrödinger, LLC, New York, NY, 2015) from the Maestro interface (Maestro, version 10.4; Schrödinger, LLC, New York, NY, 2015). Water molecules and other HET atoms were deleted. The structures of investigated compounds were built by 2D sketcher of Maestro, then these 2D structures were prepared by LigPrep (LigPrep, version 3.6; Schrödinger, LLC: New York, NY, 2015), and their protonation states were generated at pH 7.0 ± 2.0 using Epik (Epik, version 3.4; Schrödinger, LLC: New York, NY, 2015). The binding site of initial

glide docking was defined by the centroid of the ALY and the inner- and outer-box dimensions were 10 Å × 10 Å × 10 Å and 20 Å × 20 Å × 20 Å, respectively. An energy window of 2.5 kcal/mol was applied for ring conformations sampling of the investigated compounds; conformations including nonplanar feature of amide bonds were penalized. When the initial docking (Standard Precision Mode) was performed using Glide software (Glide, version 6.9; Schrödinger, LLC: New York, NY, 2015), side-chains of residues within a shell of 5 Å around each ligand were refined and optimized by Prime (version 4.2, Schrödinger, LLC, New York, NY, 2015). Then investigated compounds were redocked into the lowest energy structure within 30 kcal/mol. Top 20 poses were exported for each ligand for visual inspection and further analysis.

***Colony formation assay***

HCT116 cells were plated in 6-well plates in a volume of 2 mL and treated with compounds in corresponding concentration (DMSO as control) for 14 days. The supernatant was removed and the cells were washed using PBS buffer. Then the colonies were stained by 0.1% crystal violet for 30 min. The number of colonies were counted.

***Western Blot Analysis***

Total cell lysates were separated by 4%-16% SDS-polyacrylamide gels and transferred to nitrocellulose membranes. The blots were blocked with blocking buffer (5% nonfat milk in PBST) for 30-60 min at room temperature and incubated with primary antibodies overnight at 4°C. Then the blots were washed three times with PBST and incubated with 1:10000 dilution of donkey anti-rabbit secondary antibody (HRP conjugated) for 1 h. Followed by another three washes, bands were detected in a ChemiScope3400 imaging system using ECL substrate (Clinx).

Quantitative real time PCR

Total RNA was isolated from cells using TRIzol Reagent (Life Technologies) following the manufacturer's instructions. cDNA was obtained by reverse transcription using HiScript II Q RT SuperMix (Vazyme Biotech). QRT-PCR was performed using AceQ qPCR SYBR Green Master Mix (Vazyme Biotech) and detected by Quant Studio 6 Flex Real-Time PCR system (ABI). GAPDH was used as an internal control. Fold change of gene expression data was calculated by using of the ΔΔCt

= ΔCt (GENE-GAPDH)normal – ΔCt (GENE-GAPDH)cancer method. All Samples were run in triplicates and results were presented as mean ± SD. Detailed sequence of the primers used in the experiments can be found in the Supporting Information.

# ASSOCIATED CONTENT

***Supporting Information***

The process of setting up AlphaScreen assay, the compound with high activity in second round screening, the enzymatic selectivity of compound DC_M01_7, the result of MG149 in radioactive acetylation assay, the cell viability assay of DC_M01_7 and MG149, primers used in qRT-PCR, the spectral and analytical data of all compounds and copies of $^{1}$H NMR and $^{13}$C NMR spectra of all compounds are in supporting in information.

# AUTHOR INFORMATION

***Corresponding Authors***

*H.L.: telephone, 86-21-50806600; e-mail, hliu@simm.ac.cn

*C.L.: telephone, 86-21-50806600; e-mail, cluo@simm.ac.cn.

***Author Contributions***

#R.Z., J.W. contributed equally to this work.

# ACKNOWLEDGMENTS

This work was supported by the Major Project of Chinese National Programs for Fundamental Research and Development (2015CB910304), the National Natural Science Foundation of China (21472209, 81625022, 21472208, and 81430084), and Chinese Academy of Sciences (XDA12020353)

# ABBREVIATIONS USED

μ, micro; μM, micromole per liter; °C, degrees celsius; HEPES, 4-(2-hydroxyethyl)-1-piperazineethanesulfonic acid; $IC_{50}$, half-maximum inhibitory concentration; IPTG, isopropyl β-D-1-thiogalactopyranoside; Kd, equilibrium dissociation constant; LB, Luria−Bertani; mM, millimole per liter; min, minute; nM, nanomole per liter

# REFERENCES

[1] C.E. Brown, T. Lechner, L. Howe, J.L. Workman, The many HATs of transcription coactivators, Trends in Biochemical Sciences, 25 (2000) 15-19.

[2] A. Kimura, K. Matsubara, M. Horikoshi, A decade of histone acetylation: marking eukaryotic chromosomes with specific codes, Journal of biochemistry, 138 (2005) 647-662.

[3] M. Shogren-Knaak, H. Ishii, J.-M. Sun, M.J. Pazin, J.R. Davie, C.L. Peterson, Histone H4-K16 Acetylation Controls Chromatin Structure and Protein Interactions, Science, 311 (2006) 844.

[4] C.R. Hunt, D. Ramnarain, N. Horikoshi, P. Iyengar, R.K. Pandita, J.W. Shay, T.K. Pandita, Histone modifications and DNA double-strand break repair after exposure to ionizing radiations, Radiation research, 179 (2013) 383-392.

[5] E.R. Smith, C. Cayrou, R. Huang, W.S. Lane, J. Côté, J.C. Lucchesi, A Human Protein Complex Homologous to the Drosophila MSL Complex Is Responsible for the Majority of Histone H4 Acetylation at Lysine 16, Molecular and cellular biology, 25 (2005) 9175-9188.

[6] F. Manzo, F.P. Tambaro, A. Mai, L. Altucci, Histone acetyltransferase inhibitors and preclinical studies, Expert opinion on therapeutic patents, 19 (2009) 761-774.

[7] A. Gupta, T.G. Guerin-Peyrou, G.G. Sharma, C. Park, M. Agarwal, R.K. Ganju, S. Pandita, K. Choi, S. Sukumar, R.K. Pandita, T. Ludwig, T.K. Pandita, The mammalian ortholog of Drosophila MOF that acetylates histone H4 lysine 16 is essential for embryogenesis and oncogenesis, Molecular and cellular biology, 28 (2008) 397-409.

[8] L. Zhao, D.L. Wang, Y. Liu, S. Chen, F.L. Sun, Histone acetyltransferase hMOF promotes S phase entry and tumorigenesis in lung cancer, Cellular signalling, 25 (2013) 1689-1698.

[9] Q. Li, H. Sun, Y. Shu, X. Zou, Y. Zhao, C. Ge, hMOF (human males absent on the first), an oncogenic protein of human oral tongue squamous cell carcinoma, targeting EZH2 (enhancer of zeste homolog 2), Cell Prolif, 48 (2015) 436-442.

[10] A.C. Carrano, E. Eytan, A. Hershko, M. Pagano, SKP2 is required for ubiquitin-mediated degradation of the CDK inhibitor p27, Nature Cell Biology, 1 (1999) 193.

[11] Z. Chen, X. Ye, N. Tang, S. Shen, Z. Li, X. Niu, S. Lu, L. Xu, The histone acetylranseferase hMOF acetylates Nrf2 and regulates anti-drug responses in human non-small cell lung cancer, British journal of pharmacology, 171 (2014) 3196-3211.

[12] D. You, H. Zhao, Y. Wang, Y. Jiao, M. Lu, S. Yan, Acetylation Enhances the Promoting Role of AIB1 in Breast Cancer Cell Proliferation, Mol Cells, 39 (2016) 663-668.

[13] M.P. Bhadra, N. Horikoshi, S.N. Pushpavallipvalli, A. Sarkar, I. Bag, A. Krishnan, J.C. Lucchesi, R. Kumar, Q. Yang, R.K. Pandita, M. Singh, U. Bhadra, J.C. Eissenberg, T.K. Pandita, The role of MOF in the ionizing radiation response is conserved in Drosophila melanogaster, Chromosoma, 121 (2012) 79-90.

[14] K. Pruitt, R.L. Zinn, J.E. Ohm, K.M. McGarvey, S.-H.L. Kang, D.N. Watkins, J.G. Herman, S.B. Baylin, Inhibition of SIRT1 Reactivates Silenced Cancer Genes without Loss of Promoter DNA Hypermethylation, PLoS genetics, 2 (2006) e40.

[15] A. Okonkwo, J. Mitra, G.S. Johnson, L. Li, W.M. Dashwood, M. Hegde, C. Yue, R.H. Dashwood, P. Rajendran, Heterocyclic Analogs of Sulforaphane Trigger DNA Damage and Impede DNA Repair in Colon Cancer Cells: Interplay of HATs and HDACs, Mol Nutr Food Res, (2018) e1800228.

[16] G. Dumbovic, J. Biayna, J. Banus, J. Samuelsson, A. Roth, S. Diederichs, S. Alonso, M. Buschbeck, M.

Perucho, S.V. Forcales, A novel long non-coding RNA from NBL2 pericentromeric macrosatellite forms a perinucleolar aggregate structure in colon cancer, Nucleic Acids Res, 46 (2018) 5504-5524.

[17] F. Bishehsari, P.A. Engen, N.Z. Preite, Y.E. Tuncil, A. Naqib, M. Shaikh, M. Rossi, S. Wilber, S.J. Green, B.R. Hamaker, K. Khazaie, R.M. Voigt, C.B. Forsyth, A. Keshavarzian, Dietary Fiber Treatment Corrects the Composition of Gut Microbiota, Promotes SCFA Production, and Suppresses Colon Carcinogenesis, Genes (Basel), 9 (2018).

[18] D.G. Valerio, H. Xu, C.W. Chen, T. Hoshii, M.E. Eisold, C. Delaney, M. Cusan, A.J. Deshpande, C.H. Huang, A. Lujambio, Y.G. Zheng, J. Zuber, T.K. Pandita, S.W. Lowe, S.A. Armstrong, Histone Acetyltransferase Activity of MOF Is Required for MLL-AF9 Leukemogenesis, Cancer research, 77 (2017) 1753-1762.

[19] W. Lu, R. Zhang, H. Jiang, H. Zhang, C. Luo, Computer-Aided Drug Design in Epigenetics, Frontiers in chemistry, 6 (2018) 57.

[20] H. Wapenaar, F.J. Dekker, Histone acetyltransferases: challenges in targeting bi-substrate enzymes, Clinical epigenetics, 8 (2016) 59.

[21] A.N. Poux, M. Cebrat, C.M. Kim, P.A. Cole, R. Marmorstein, Structure of the GCN5 histone acetyltransferase bound to a bisubstrate inhibitor, Proceedings of the National Academy of Sciences of the United States of America, 99 (2002) 14065-14070.

[22] K. Balasubramanyam, V. Swaminathan, A. Ranganathan, T.K. Kundu, Small molecule modulators of histone acetyltransferase p300, The Journal of biological chemistry, 278 (2003) 19134-19140.

[23] K. Balasubramanyam, M. Altaf, R.A. Varier, V. Swaminathan, A. Ravindran, P.P. Sadhale, T.K. Kundu, Polyisoprenylated benzophenone, garcinol, a natural histone acetyltransferase inhibitor, represses chromatin transcription and alters global gene expression, The Journal of biological chemistry, 279 (2004) 33716-33726.

[24] K. Balasubramanyam, R.A. Varier, M. Altaf, V. Swaminathan, N.B. Siddappa, U. Ranga, T.K. Kundu, Curcumin, a novel p300/CREB-binding protein-specific inhibitor of acetyltransferase, represses the acetylation of histone/nonhistone proteins and histone acetyltransferase-dependent chromatin transcription, The Journal of biological chemistry, 279 (2004) 51163-51171.

[25] M. Biel, A. Kretsovali, E. Karatzali, J. Papamatheakis, A. Giannis, Design, synthesis, and biological evaluation of a small-molecule inhibitor of the histone acetyltransferase Gcn5, Angewandte Chemie, 43 (2004) 3974-3976.

[26] L. Stimson, M.G. Rowlands, Y.M. Newbatt, N.F. Smith, F.I. Raynaud, P. Rogers, V. Bavetsias, S. Gorsuch, M. Jarman, A. Bannister, T. Kouzarides, E. McDonald, P. Workman, G.W. Aherne, Isothiazolones as inhibitors of PCAF and p300 histone acetyltransferase activity, Molecular Cancer Therapeutics, 4 (2005) 1521.

[27] K. Mantelingu, B.A.A. Reddy, V. Swaminathan, A.H. Kishore, N.B. Siddappa, G.V.P. Kumar, G. Nagashankar, N. Natesh, S. Roy, P.P. Sadhale, U. Ranga, C. Narayana, T.K. Kundu, Specific Inhibition of p300-HAT Alters Global Gene Expression and Represses HIV Replication, Chemistry & biology, 14 (2007) 645-657.

[28] A. Mai, D. Rotili, D. Tarantino, P. Ornaghi, F. Tosi, C. Vicidomini, G. Sbardella, A. Nebbioso, M. Miceli, L. Altucci, P. Filetici, Small-Molecule Inhibitors of Histone Acetyltransferase Activity: Identification and Biological Properties, Journal of Medicinal Chemistry, 49 (2006) 6897-6907.

[29] A.T. Smith, M.R. Livingston, A. Mai, P. Filetici, S.F. Queener, W.J. Sullivan, Quinoline Derivative MC1626,

a Putative GCN5 Histone Acetyltransferase (HAT) Inhibitor, Exhibits HAT-Independent Activity against Toxoplasma gondii, Antimicrobial Agents and Chemotherapy, 51 (2007) 1109-1111.

[30] A. Mai, D. Rotili, D. Tarantino, A. Nebbioso, S. Castellano, G. Sbardella, M. Tini, L. Altucci, Identification of 4-hydroxyquinolines inhibitors of p300/CBP histone acetyltransferases, Bioorganic & Medicinal Chemistry Letters, 19 (2009) 1132-1135.

[31] M. Ghizzoni, J. Wu, T. Gao, H.J. Haisma, F.J. Dekker, Y. George Zheng, 6-alkylsalicylates are selective Tip60 inhibitors and target the acetyl-CoA binding site, European journal of medicinal chemistry, 47 (2012) 337-344.

[32] H. Xiong, J. Han, J. Wang, W. Lu, C. Wang, Y. Chen, L. Fulin, N. Zhang, Y.C. Liu, C. Zhang, H. Ding, H. Jiang, W. Lu, C. Luo, B. Zhou, Discovery of 1,8-acridinedione derivatives as novel GCN5 inhibitors via high throughput screening, European journal of medicinal chemistry, 151 (2018) 740-751.

[33] Y. Feng, S. Xiao, Y. Chen, H. Jiang, N. Liu, C. Luo, S. Chen, H. Chen, Design, synthesis and biological evaluation of benzo[cd]indol-2(1H)-ones derivatives as BRD4 inhibitors, European journal of medicinal chemistry, 152 (2018) 264-273.

[34] T. Lu, J.-c. Hu, W.-c. Lu, J. Han, H. Ding, H. Jiang, Y.-y. Zhang, L.-y. Yue, S.-j. Chen, H.-l. Jiang, K.-x. Chen, H.-f. Chai, C. Luo, Identification of small molecule inhibitors targeting the SMARCA2 bromodomain from a high-throughput screening assay, Acta Pharmacologica Sinica, (2018).

[35] J. Xing, W. Lu, R. Liu, Y. Wang, Y. Xie, H. Zhang, Z. Shi, H. Jiang, Y.-C. Liu, K. Chen, H. Jiang, C. Luo, M. Zheng, Machine-Learning-Assisted Approach for Discovering Novel Inhibitors Targeting Bromodomain-Containing Protein 4, Journal of Chemical Information and Modeling, 57 (2017) 1677-1690.

[36] A. Gupta, T.G. Guerin-Peyrou, G.G. Sharma, C. Park, M. Agarwal, R.K. Ganju, S. Pandita, K. Choi, S. Sukumar, R.K. Pandita, T. Ludwig, T.K. Pandita, The Mammalian Ortholog of Drosophila MOF That Acetylates Histone H4 Lysine 16 Is Essential for Embryogenesis and Oncogenesis, Molecular and cellular biology, 28 (2008) 397-409.

[37] J.A. Aglipay, S.W. Lee, S. Okada, N. Fujiuchi, T. Ohtsuka, J.C. Kwak, Y. Wang, R.W. Johnstone, C. Deng, J. Qin, T. Ouchi, A member of the Pyrin family, IFI16, is a novel BRCA1-associated protein involved in the p53-mediated apoptosis pathway, Oncogene, 22 (2003) 8931-8938.

[38] H. Xin, J. Curry, R.W. Johnstone, B.J. Nickoloff, D. Choubey, Role of IFI 16, a member of the interferon-inducible p200-protein family, in prostate epithelial cellular senescence, Oncogene, 22 (2003) 4831-4840.

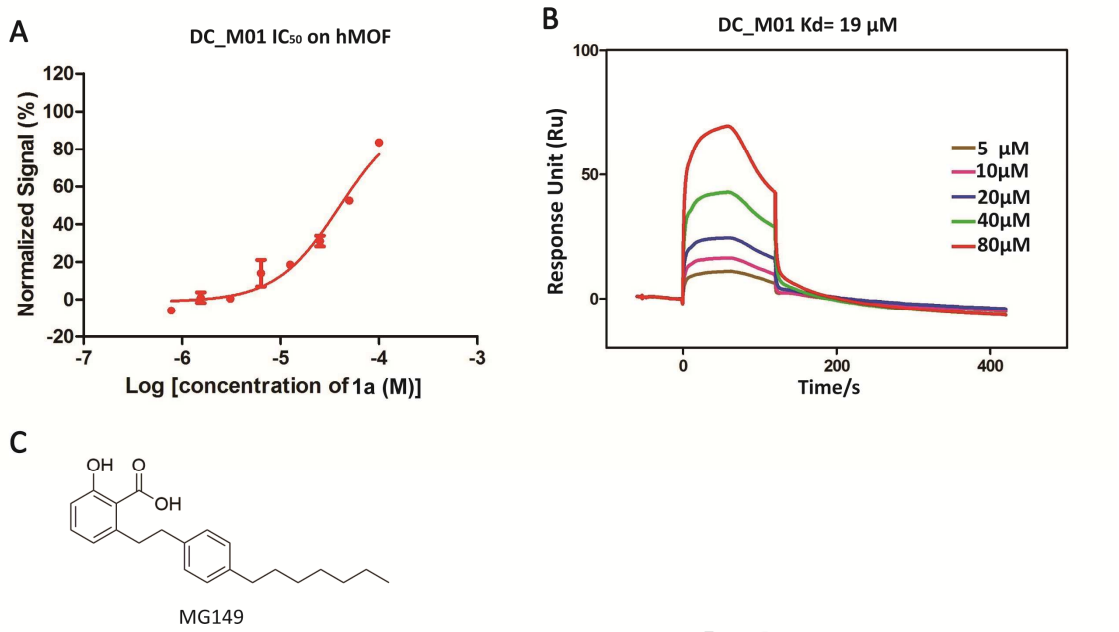


**Figure 1.** DC_M01 can inhibit hMOF in vivo and also can directly bind to hMOF. (A) The hit DC_M01 was measured by radioactive assay on hMOF with an $IC_{50}$ of 40 μM. (B) The $K_d$ of DC_M01 was determined using SPR as 19 μM. (C) The chemical structure of MG149

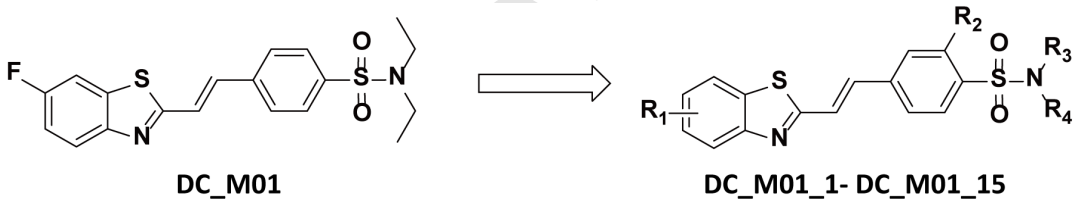


**Figure 2.** Design novel hMOF inhibitors.

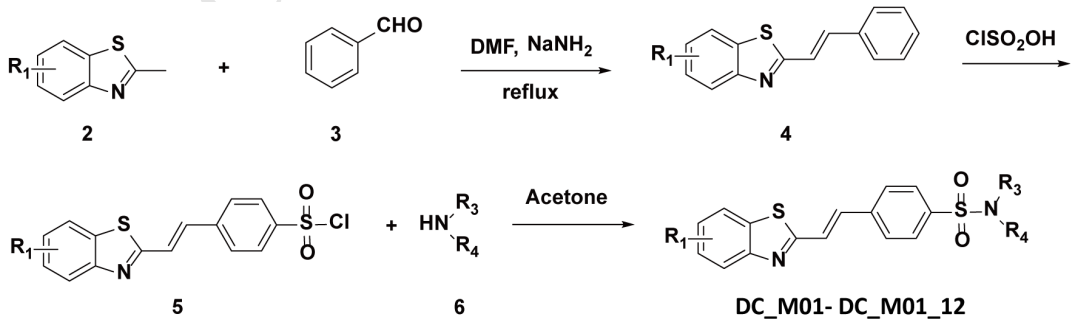

**Scheme 1.** General synthetic route to the target compounds DC_M01-DC_M01_12.

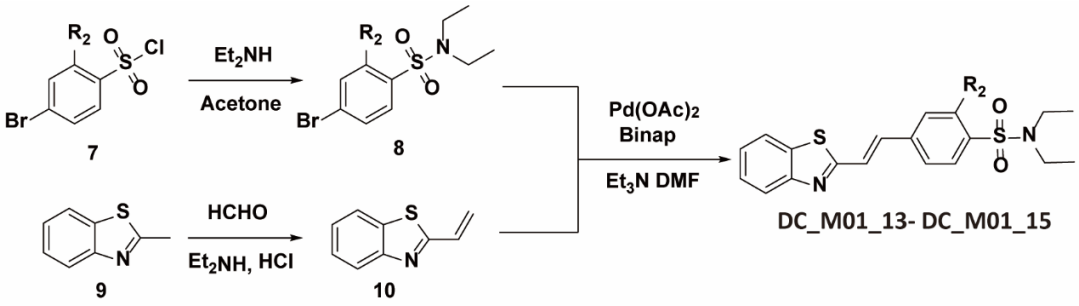


**Scheme 2.** Synthetic routes to compounds DC_M01_13-DC_M01_15

**Table 1.** The structure and inhibitory activity of DC_M01 and its analogs

| Compd. | $R_1$ | $R_2$ | $R_3$ | $R_4$ | Inh% (50 μM) | Inh% (100 μM) | $IC_{50}$ (μM) |
|---|---|---|---|---|---|---|---|
| **DC_M01** | 5-F | H | Et | Et | 53 | 84 | 40 |
| **DC_M01_1** | 5-Cl | H | Et | Et | 64 | 89 | 30 |
| **DC_M01_2** | 5-Br | H | Et | Et | 57 | 82 | 30 |
| **DC_M01_3** | 5-Me | H | Et | Et | 0 | 14 | - |
| **DC_M01_4** | 5-OMe | H | Et | Et | 14 | 13 | - |
| **DC_M01_5** | 6-Br | H | Et | Et | 5 | 21 | - |
| **DC_M01_6** | 5,6-*di*-Me | H | Et | Et | 95 | 96 | 7.7 |
| **DC_M01_7** | H | H | Et | Et | 93 | 100 | 6 |
| **DC_M01_8** | H | H | Me | Me | 9 | 14 | - |
| **DC_M01_9** | H | H | Ph | H | 13 | 25 | - |
| **DC_M01_10** | H | H | Bn | H | 1 | 11 | - |
| **DC_M01_11** | H | H | 4-Me-$PhCH_2$ | H | 17 | 33 | - |
| **DC_M01_12** | H | H | 4-OMe-$PhCH_2$ | H | 0 | 28 | - |
| **DC_M01_13** | H | F | Et | Et | 16 | 18 | - |
| **DC_M01_14** | H | Cl | Et | Et | 7 | 12 | - |
| **DC_M01_15** | H | Me | Et | Et | 28 | 30 | - |
| **MG149** | | | - | | 100 | 100 | 15 |

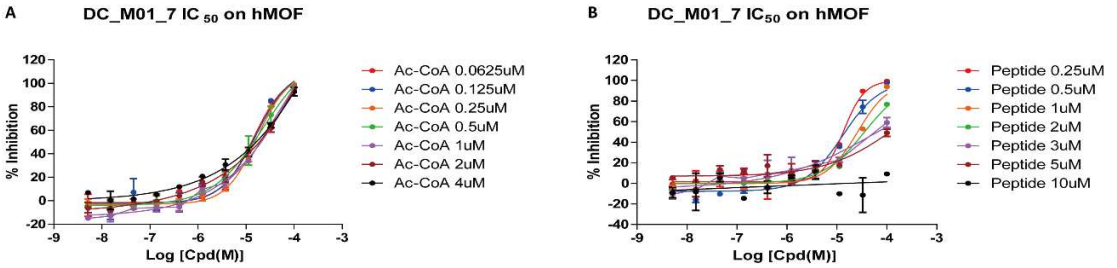


**Figure 3.** DC_M01_7 $IC_{50}$ on hMOF in radioactive competitive assay. (A) The $IC_{50}$ of DC_M01_7 did not alter when changing the concentration of acetyl coenzyme A. (B) The $IC_{50}$ of DC_M01_7 decreased when increasing the concentration of histone 4 peptide.

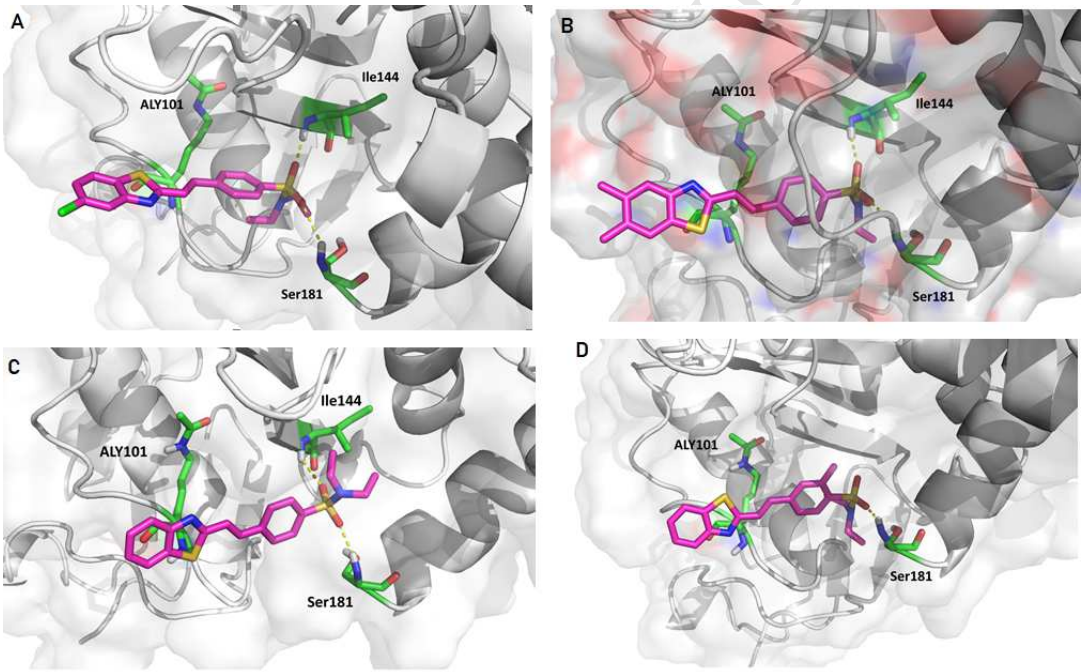


**Figure 4**. (A) The binding mode of DC_M01 in the active site of hMOF. (B) The binding mode of DC_M01_6 in the active site of hMOF. (C) The binding mode of DC_M01_7 in the active site of hMOF. (D) The binding mode of DC_M01_15 in the active site of hMOF. All figures were prepared using PyMol (http://www.pymol.org/).

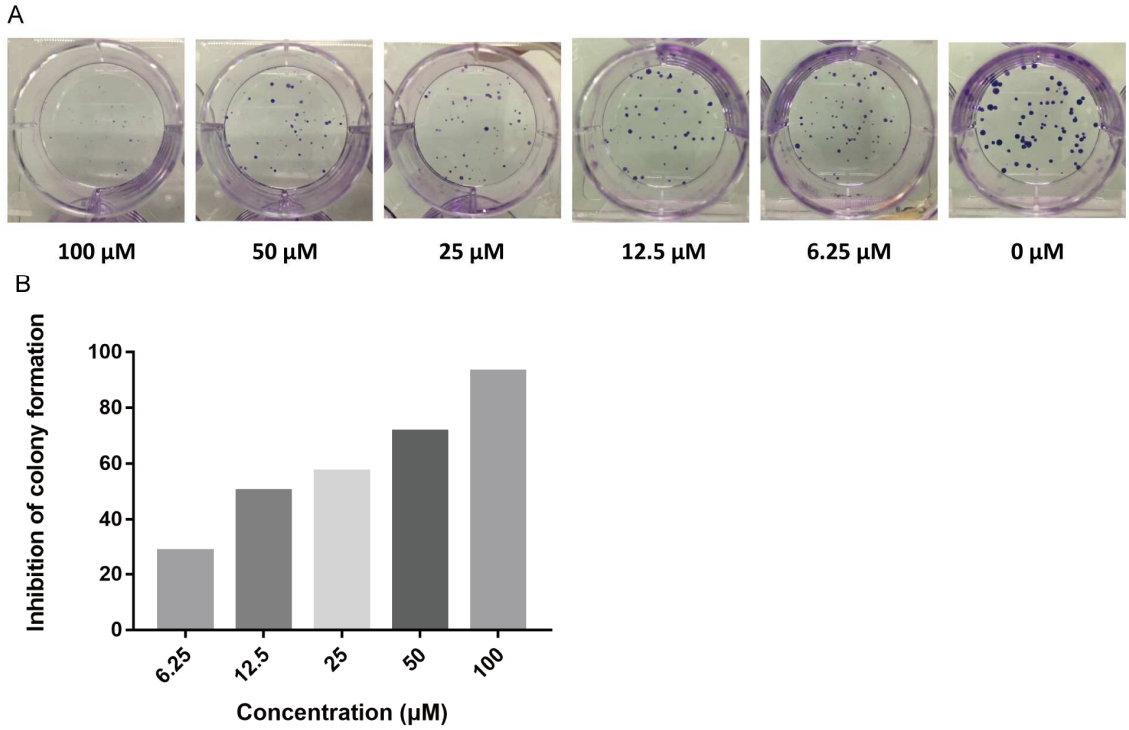


**Figure 5.** (A-B) DC_M01_7 was diluted to different concentrations from 100 μM to 6.25 μM to treat HCT116 cells. The same volume DMSO is used as control group. Colonies were counted and pictured. The inhibition rate of DC_M01_7 was calculated and pictured.

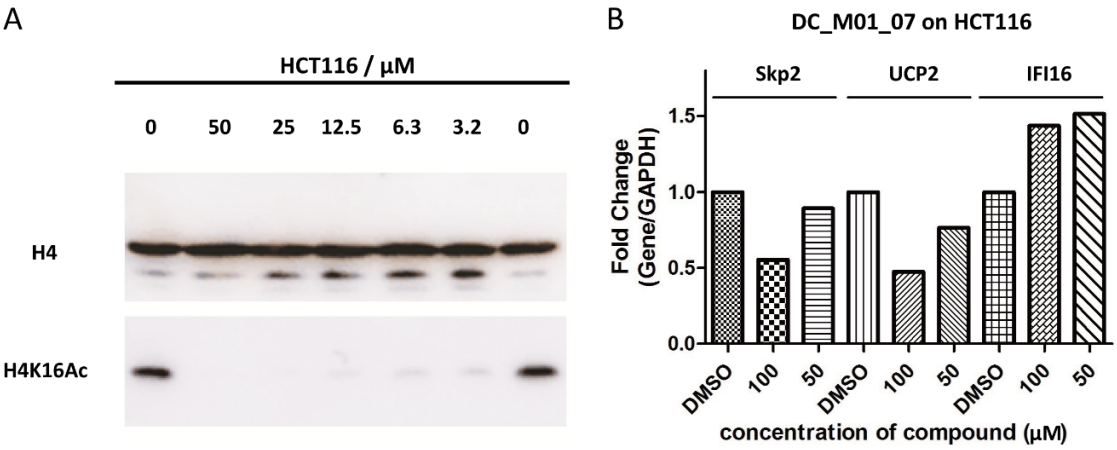

**Figure 6.** Effect of DC_M01_7 on H4K16 acetylation and related genes' expression in HCT116. (A) DC_M01_7 can dose-dependently inhibit the acetylation of H4K16 acetylation. (B) DC_M01_7 can decrease the expression of SKP2 and UCP2 and elevate the expression of IFI16.

## HIGHLIGHT

- We identified a potent hMOF inhibitor with a new scaffold using high throughput screening.
- The binding affinity of the hit compound DC_M01 was measured by SPR.
- DC_M01_7, which was obtained by chemical modification, could inhibit hMOF activity in a substrate competitive mode.
- DC_M01_7 could inhibit hMOF activity in HCT116 cells and regulate downstream genes.